Chapter 2

FINITE VOLUME METHODS AND THE WAVE PROPAGATION ALGORITHM

The goal of this thesis is to present an algorithm to solve hyperbolic conservation laws on smooth curved manifolds. It was stated in Chapter 1 that physical systems described by the integral conservation law (1.1) may have discontinuous solutions that satisfy a weak form of the PDE (1.2). A numerical method that will be useful for conservation laws with strong discontinuities on curved manifolds must have the following characteristics:

1. The algorithm must sharply resolve discontinuities without introducing oscillations while producing an accurate solution in smooth regions.

2. Since many of the systems of interest are nonlinear, shock speeds must be approximated accurately. It follows that physically conserved quantities must be numerically conserved.

3. Geometry will play a significant roll in the structure of the solution (i.e. in the vicinity of a black hole), so the method must handle a variety of geometries in a robust manner.

As discussed in the previous chapter, second order finite difference methods do not satisfy this set of characteristics due to the oscillations they produce near discontinuities. High resolution finite volume methods, however, have been used for decades now to produce non oscillatory solutions in the vicinity of strong discontinuities, while providing high accuracy in smooth regions of the solution [15], [27], [83]. The main contribution of this thesis is to incorporate the third characteristic, the ability to handle geometry in a robust way.

One particular class of finite volume algorithms developed by LeVeque [39], [42], [44], is based on the propagation of waves. In this chapter we introduce the wave propagation algorithm as developed in [42] and [44]. Chapters that follow extend this class of high resolution algorithms to solve hyperbolic conservation laws on general smooth manifolds.

2.1 Finite volume methods

Most finite volume methods are developed for grid volumes covered by a Cartesian basis. In order to keep consistent with notation for a general basis on manifolds discussed in Chapters 5, 6, and 8, we often denote a Cartesian basis by $\{\vec{e}_{(1)}, \vec{e}_{(2)}\}$ with $(x, y) = (x^1, x^2)$ in two spatial dimensions, or $\{\vec{e}_{(1)}, \vec{e}_{(2)}, \vec{e}_{(3)}\}$ with $(x, y, z) = (x^1, x^2, x^3)$ in three dimensions. We take $\vec{e}_{(1)} = \vec{e}_{(x)}$ and $x^1 = x$ when we discuss one-dimensional problems.

Finite volume methods are based on subdividing a computational volume into *finite volume* grid cells. At a time t_n, components of $\boldsymbol{q}$ are averaged onto the grid resulting in a

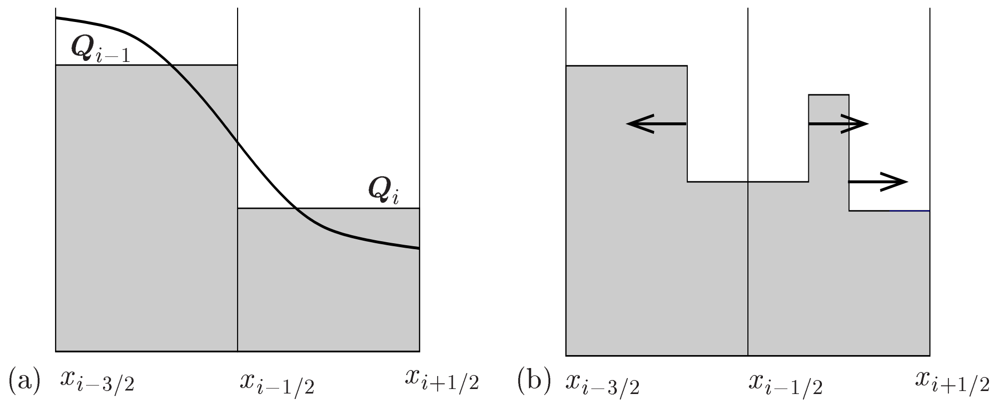

Figure 2.1: (a) The result of averaging $\boldsymbol{q}$ onto a one-dimensional finite volume grid. (b) Waves emanate from finite volume cell edges.

piece-wise constant representation of each state variable. Let $\boldsymbol{Q}_i^n$ represent an approximation to the cell average

$$\boldsymbol{Q}_i^n \approx \frac{1}{\Delta x}\int_{x_{i-1/2}}^{x_{i+1/2}} q(t_n, x)\,dx \equiv \frac{1}{\Delta x}\int_{\mathcal{C}_i} q(t_n, x)\,dx, \tag{2.1}$$

where we denote the one-dimensional finite volume cell of length $\Delta x = x_{i+1/2} - x_{i-1/2}$ by

$$\mathcal{C}_i = (x_{i-1/2}, x_{i+1/2}). \tag{2.2}$$

The finite volume approximation, $\boldsymbol{Q}_i^n$, of a smooth function is shown in Figure 2.1(a).

At the beginning of each time step, the piece-wise constant representation $\boldsymbol{Q}_i^n$ sets up unsteady *Riemann* problems at each grid cell boundary. These Riemann problems decay, inducing flux through cell boundaries throughout the time step. Figure 2.1(b) shows the cell boundary at $x_{i-1/2}$ where the initial discontinuity $\boldsymbol{Q}_i^n - \boldsymbol{Q}_{i-1}^n$ has decayed producing flux through the cell boundary. Directly computing the averaged solution at the end of the time step may be complicated due to the fact that information traveling from the left edge of the cell may be interacting with the information traveling from the right edge. This interaction will in general be non-trivial for nonlinear systems.

Instead of directly averaging the solution at the end of the time step, we integrate the one-dimensional version of equation (1.1) in time from t_n to $t_{n+1} = t_n + \Delta t$ to get

$$\begin{aligned}\int_{\mathcal{C}_i} \boldsymbol{q}(t_{n+1}, x)\,dx = &\int_{\mathcal{C}_i} \boldsymbol{q}(t_n, x)\,dx \\ &- \left(\int_{t_n}^{t_{n+1}} \boldsymbol{f}(\boldsymbol{q}(t_n, x_{i+1/2}))\,dt - \int_{t_n}^{t_{n+1}} \boldsymbol{f}(\boldsymbol{q}(t_n, x_{i-1/2}))\,dt\right).\end{aligned} \tag{2.3}$$

This relates the integral of $\boldsymbol{q}$ over $\mathcal{C}_i$ at t_{n+1}, the end of the time step, to what it was at t_n modified by the time integral of the flux at each cell boundary. With a good approximation to the *numerical flux* defined by

$$\boldsymbol{F}^n_{i-1/2} \approx \frac{1}{\Delta t}\int_{t_n}^{t_{n+1}} \boldsymbol{f}(\boldsymbol{q}(t, x_{i-1/2}))\,dt, \tag{2.4}$$

an explicit numerical method follows from (2.3). Many different numerical flux functions can be found in the literature [17], [18], [27], [69]. We discuss approximations to numerical flux functions in Appendix A. Using the numerical flux (2.4), together with (2.1), we can write (2.3) as

$$\boldsymbol{Q}^{n+1}_i = \boldsymbol{Q}^n_i - \frac{\Delta t}{\Delta x}\left(\boldsymbol{F}^n_{i+1/2} - \boldsymbol{F}^n_{i-1/2}\right), \tag{2.5}$$

which is the typical form of a finite volume numerical method based on flux differences.

The numerical method (2.5) has the property that if

$$\boldsymbol{F}^n_{i+1/2} = \boldsymbol{F}^n_{i-1/2}, \tag{2.6}$$

meaning that what is flowing in one side of the cell is flowing out the other side, then the finite volume approximation $\boldsymbol{Q}^n_i$ remains unchanged over the time step. In fact, update (2.5) exactly conserves $\boldsymbol{Q}^n_i$ at each time step since on a grid with N cells we have

$$\begin{aligned}\sum_{i=1}^{N}\boldsymbol{Q}^{n+1}_i &= \sum_{i=1}^{N}\boldsymbol{Q}^n_i - \frac{\Delta t}{\Delta x}\left(-\boldsymbol{F}^n_{1-1/2} + \text{telescoping terms} + \boldsymbol{F}^n_{N+1/2}\right)\\ &= \sum_{i=1}^{N}\boldsymbol{Q}^n_i - \frac{\Delta t}{\Delta x}\left(-\boldsymbol{F}^n_{1-1/2} + \boldsymbol{F}^n_{N+1/2}\right),\end{aligned} \tag{2.7}$$

which states that the numerical solution over a time step is only affected by the flux at grid boundaries. This is a very desirable discrete representation of the conservative properties of the conservation law (1.1).

2.2 The Riemann problem

In one space dimension with $x^1 = x$, the conservation law (1.3) has the form

$$\boldsymbol{q}_{,t} + \boldsymbol{f}(\boldsymbol{q})_{,x} = 0. \tag{2.8}$$

A Riemann problem consists of this hyperbolic PDE together with piecewise constant initial data having a single jump discontinuity at $x = 0$,

$$\boldsymbol{q}(t=0, x) = \begin{cases}\boldsymbol{q}_l & \text{if } x < 0\\ \boldsymbol{q}_r & \text{if } x > 0.\end{cases} \tag{2.9}$$

The jump discontinuity can be placed at any $x = X$, but without loss of generality we take $X = 0$. When f is a linear function of q the initial discontinuity breaks up and travels along characteristics of the equation. The solution involves piece-wise constant states separated by waves carrying part of the original jump discontinuity. The solution to a Riemann problem for a general constant-coefficient linear system is presented in Section 2.2.1. We are interested in the linear solution because nonlinear systems are often locally linearized, resulting in a linear Riemann problem.

Solutions to Riemann problems for equations with nonlinear flux functions are more complicated. The solution still consists of piece-wise constant states separated by waves, but the waves can be genuinely nonlinear discontinuities (shock waves), smooth rarefaction waves, or linearly degenerate discontinuities (contact waves). We briefly describe the nonlinear waves in Section 2.2.2. Many more details about both linear and nonlinear systems with examples can be found in [43], [46], [48].

2.2.1 Linear systems

Consider a linear flux function

$$\boldsymbol{f}(\boldsymbol{q}) = A\,\boldsymbol{q}, \tag{2.10}$$

where $A \in \mathbb{R}^{n_{\mathrm{eq}} \times n_{\mathrm{eq}}}$ is a diagonalizable constant coefficient matrix with real eigenvalues. Using this flux function in equation (2.8) we get

$$\boldsymbol{q}_{,t} + A\,\boldsymbol{q}_{,x} = 0. \tag{2.11}$$

This linear PDE is hyperbolic and since A is diagonalizable, we can write $\mathbf{A}_x = \mathbf{R}\Lambda\mathbf{R}^{-1}$, where

$$R = \left(\boldsymbol{r}^1 \middle| \cdots \middle| \boldsymbol{r}^{n_{eq}}\right), \quad \Lambda = \mathrm{diag}(\lambda^1, \cdots, \lambda^{n_{eq}}), \quad R^{-1} = \begin{pmatrix} \boldsymbol{l}^1 \\ - \\ \vdots \\ - \\ \boldsymbol{l}^{n_{eq}} \end{pmatrix}. \tag{2.12}$$

The right eigenvectors, $\boldsymbol{r}^i$, and left eigenvectors, $\boldsymbol{l}^j$, satisfy the relationship $\boldsymbol{l}^j \cdot \boldsymbol{r}^i = \delta^{ij}$, and we order the eigenvalues such that $\lambda^1 \leq \lambda^2 \leq \cdots \leq \lambda^{n_{eq}}$.

Now consider a Riemann problem for the system (2.11) with the discontinuity placed at $X = 0$. Since the system is linear, the discontinuity will propagate along characteristics of (2.11). Transforming to *characteristic* variables defined by

$$\boldsymbol{w} = R^{-1}\,\boldsymbol{q}, \tag{2.13}$$

we can write equation (2.11) as

$$\boldsymbol{w}_{,t} + \Lambda\,\boldsymbol{w}_{,1} = 0, \tag{2.14}$$

which is a set of uncoupled advection equations for the components of $\boldsymbol{w}$. We also project both $\boldsymbol{q}_l$ and $\boldsymbol{q}_r$ onto the set of right eigenvectors so that

$$\begin{aligned} \boldsymbol{q}_l &= R\,\boldsymbol{w}_l = \sum_{p=1}^{n_{eq}} w_l^p \boldsymbol{r}^p \\ \boldsymbol{q}_r &= R\,\boldsymbol{w}_r = \sum_{p=1}^{n_{eq}} w_r^p \boldsymbol{r}^p, \end{aligned} \tag{2.15}$$

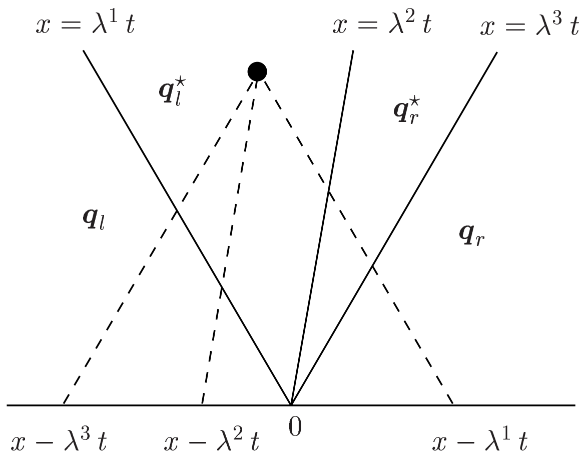

Figure 2.2: The solution for linear problems is a superposition of waves. Waves separate piece-wise constant regions of the solution.

and the initial condition for the p^{th} advection equation becomes

$$w^p(t=0,x) = \begin{cases} w_l^p & \text{if } x<0 \\ w_r^p & \text{if } x>0. \end{cases} \tag{2.16}$$

Each advection equation in (2.14) with initial data (2.16) has the solution

$$w^p(t,x) = w_l^p\,\mathcal{H}(\lambda^p t - x) + w_r^p\,\mathcal{H}(x-\lambda^p t), \tag{2.17}$$

where $\mathcal{H}(x)$ is the Heaviside function. If we define $\mathscr{P}^-$ to be the set of all p such that $\lambda^p<0$, and similarly define $\mathscr{P}^+$ to be the set such that $\lambda^p>0$, then we can transform (2.17) back using $\boldsymbol{q}=R\,\boldsymbol{w}$ to find

$$\boldsymbol{q}(t,x) = \sum_{p\in\mathscr{P}^-} w_r^p\,\boldsymbol{r}^p + \sum_{p\in\mathscr{P}^+} w_l^p\,\boldsymbol{r}^p, \tag{2.18}$$

which is the desired result. The solution is a superposition of waves traveling along characteristics of (2.11).

Figure 2.2 illustrates the construction of the solution (2.18) at a particular point in the spacetime domain. Denote the solution at this point by $\boldsymbol{q}_l^\star$ and trace back along characteristics to see what part of the initial condition affects the solution. In the figure we see that

$$\begin{aligned} \boldsymbol{q}_l^\star &= w_r^1\,\boldsymbol{r}^1 + w_l^2\,\boldsymbol{r}^2 + w_l^3\,\boldsymbol{r}^3 \\ &= \boldsymbol{q}_l + \left(w_r^1 - w_l^1\right)\,\boldsymbol{r}^1, \end{aligned} \tag{2.19}$$

so $\boldsymbol{q}_l^\star$ can be viewed as the left state modified by a left-propagating wave $\boldsymbol{\mathcal{W}}^1 = (w_r^1 - w_l^1)\,\boldsymbol{r}^1$.

It is worth noting that the Riemann solution is constant and equal to $\boldsymbol{q}_l^\star$ along the ray $x/t = 0$ in Figure 2.2. If this were the edge of a finite volume grid cell, then a very good numerical flux function $\boldsymbol{F}^n$ from (2.4) would be

$$\boldsymbol{F}^n = \boldsymbol{f}(\boldsymbol{q}_l^\star) = \boldsymbol{f}(\boldsymbol{q}_l + \boldsymbol{\mathcal{W}}^1). \tag{2.20}$$

In this special case $\boldsymbol{F}^n$ is not an approximation to the time average of the flux, but the exact value. Defining the numerical flux as the flux function evaluated at the exact solution to the Riemann problem leads to the Godunov method [27].

2.2.2 Nonlinear systems

As previously discussed, the solution to the Riemann problem for nonlinear flux functions is more complicated than the linear case. The waves generated by the decay of the initial discontinuity may be shock waves, rarefaction waves, or contact discontinuities. The type of wave generated depends on the local characteristics, which for nonlinear problems depend on the solution itself.

Consider a scalar version of equation (2.8) so that $n_{eq} = 1$. As long as $q(t, x)$ is smooth, characteristic curves $X(t)$ are defined by the quasi-linear form

$$q_{,t} + f^{'}(q)\, q_{,x} = 0. \tag{2.21}$$

These curves are defined so that $X^{'}(t) = f^{'}(q(t, X(t)))$ which leads to the fact that for (2.21) q is constant along such curves because

$$\begin{aligned} \frac{d}{dt} q(t, X(t)) &= q_{,t} + X^{'}(t)\, q_{,x} \\ &= q_{,t} + f^{'}(q)\, q_{,x} \\ &= 0. \end{aligned} \tag{2.22}$$

If q is constant, then $f^{'}(q)$ is also constant so that $X^{'}(t) = \text{const.}$ and the characteristics are straight lines.

Shock waves

Suppose $f^{'}(q)$ is a monotonically increasing function of q so that the initial conditions in Figure 2.3(a) would have $f^{'}(q_l) > f^{'}(q_r)$. In this case, the characteristics to the left and right of the initial discontinuity would be disappearing into the line $x = st$ shown in Figure 2.3(b), where s is the shock speed given by the *Rankine-Hugoniot* conditions

$$s = \frac{f(q_r) - f(q_l)}{q_r - q_l}. \tag{2.23}$$

Rarefaction waves

Initial conditions as depicted in Figure 2.4(a), however, have $f^{'}(q_l) < f^{'}(q_r)$ so that the characteristics spread as shown in Figure 2.4(b). In this case the solution remains smooth.

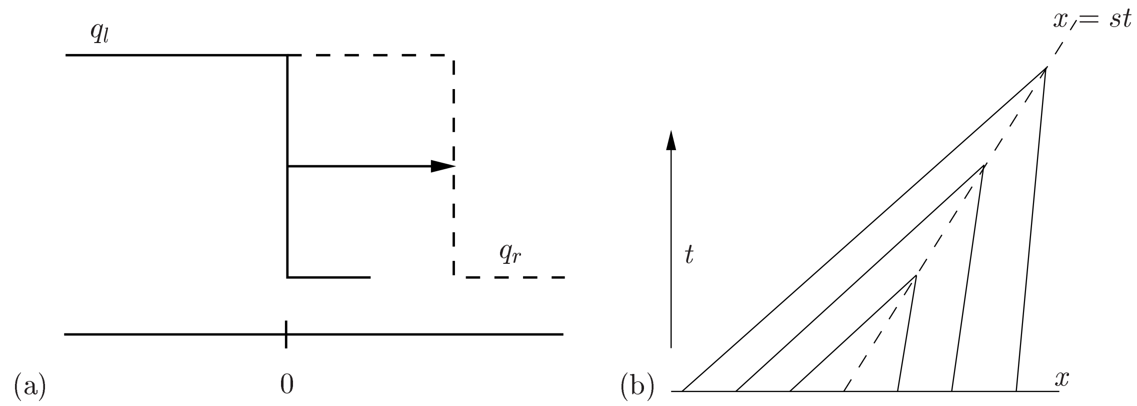

Figure 2.3: (a) The function q is constant along characteristics. (b) The initial discontinuity in q travels at speed s. Since $f'(q_l) > f'(q_r)$ the characteristics disappear into the line $x = st$.

For systems, the quasi-linear form of the conservation law becomes

$$\boldsymbol{q}_{,t} + A^k(\boldsymbol{q})\boldsymbol{q}_{,k} = 0, \tag{2.24}$$

where $A^k \to A^k(\boldsymbol{q}) \equiv \partial \boldsymbol{f}^{(k)}/\partial \boldsymbol{q}$ is now the Jacobian of the flux function $\boldsymbol{f}^{(k)}(\boldsymbol{q}) : \mathbb{R}^{n_{eq}} \to \mathbb{R}^{n_{eq}}$. Throughout this thesis, as for the linear case, we assume hyperbolicity so that each A^k has a complete set of linearly independent eigenvectors $\{\boldsymbol{r}^1, \cdots, \boldsymbol{r}^{n_{eq}}\}$ associated with which is an ordered set of real eigenvalues $\{\lambda^1, \cdots, \lambda^{n_{eq}}\}$ at each point of the solution domain.

For many nonlinear systems an exact solution to the Riemann problem like (2.18) is either not possible, or too computationally expensive. In that case an accurate and efficient approximate solution is desirable. These approximate solutions produce a wide range of numerical flux functions $\boldsymbol{F}^n$ [5], [17], [69]. We explore several approximate Riemann solvers in Appendix A used to compute numerical results that we show in most of the following chapters. For more detail about nonlinear systems, approximate Riemann solvers, and examples of nonlinear systems the reader is referred to [26], [46], [74].

2.3 Standard wave propagation

The wave propagation algorithm is an unsplit multidimensional finite volume method used to solve hyperbolic conservation laws on a Cartesian basis. So far, we have discussed finite volume methods in general, and how to use the solution of Riemann problems that arise at each cell edge to approximate the flux at these edges. We now describe the wave propagation algorithm as developed by LeVeque in [44] and [42] and how it fits into the class of finite volume methods (2.5) based on flux differences.

We begin by presenting in Section 2.3.1 the one-dimensional algorithm and show how the numerical update is constructed from waves like those discussed in Section 2.2. It is also

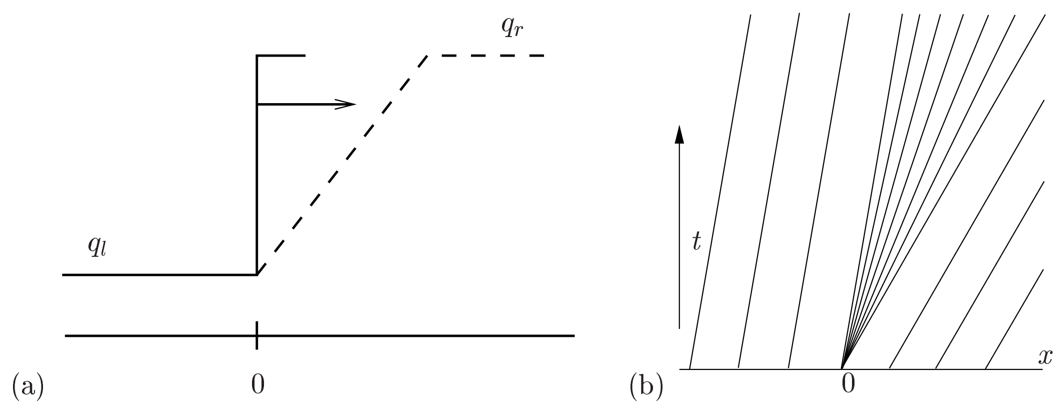

Figure 2.4: (a) The function q is still constant along characteristics. (b) The initial discontinuity in q now decomposes into a continuously varying rarefaction wave. The characteristics fan out from the location of the initial discontinuity.

shown that the update is numerically conservative. We then consider the multidimensional algorithm in Section 2.3.2.

2.3.1 One dimensional algorithm

Data at time t_n in each cell, $\mathcal{C}_i$, is represented by piece-wise constant functions $\boldsymbol{Q}_i^n$, the finite volume average (2.1). These averages define one-dimensional planar Riemann problems at each cell interface. A set of n_{eq} waves $\{\boldsymbol{\mathcal{W}}_{i-1/2}^1, \cdots \boldsymbol{\mathcal{W}}_{i-1/2}^{n_{eq}}\}$ is generated in each Riemann problem that carry the entire jump in $\boldsymbol{Q}_i^n$

$$\boldsymbol{Q}_i - \boldsymbol{Q}_{i-1} = \sum_{p=1}^{n_{eq}} \boldsymbol{\mathcal{W}}_{i-1/2}^{(p)}. \tag{2.25}$$

Each wave has an associated speed for which $s_{i-1/2}^1 < \cdots < s_{i-1/2}^{n_{eq}}$. As discussed in Section 2.2.2, the waves may be shock waves, rarefaction waves, or contact discontinuities, depending on the local characteristics.

Fluctuations defined by

$$\boldsymbol{\mathcal{A}}^{\pm}\boldsymbol{\Delta Q}_{i-1/2} = \sum_p \left[s_{i-1/2}^p\right]^{\pm} \boldsymbol{\mathcal{W}}_{i-1/2}^p, \tag{2.26}$$

are used in the cell update. In equation (2.26) we have followed the notation of [45] and used $s^+ = \max(0, s)$, $s^- = \min(s, 0)$. Figure 2.5 shows a finite volume cell being influenced by a fluctuation $\boldsymbol{\mathcal{A}}^+\boldsymbol{\Delta Q}_{i-1/2}$ traveling to the right from the left edge of the cell, and $\boldsymbol{\mathcal{A}}^-\boldsymbol{\Delta Q}_{i+1/2}$ traveling to the left from the right edge.

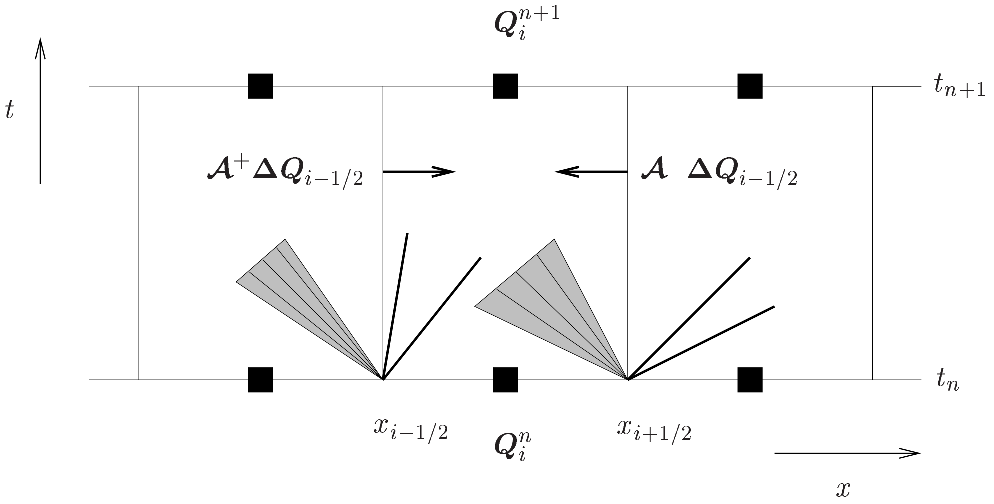

Figure 2.5: Wave generation of fluctuation differences

We motivate the use of fluctuations by considering the Taylor expansion of the constant coefficient advection equation

$$q_{,t} + u\, q_{,x} = 0, \tag{2.27}$$

which has the form

$$q(t+\Delta t) = q(t) - \Delta t\, \underbrace{u\, q_{,x}(t)}_{I} + \frac{1}{2}\Delta t^2\, \underbrace{u^2\, q_{,xx}(t)}_{II(a)} + \mathcal{O}(\Delta t^3). \tag{2.28}$$

In order to have a second order method for smooth solutions we must numerically approximate two types of terms indicated in the expansion (2.28). Type I terms are first order and we refer to them as *upwind* terms. Type II(a) terms involve the second derivative of q and will be approximated by *correction* terms.

Type I terms: upwind

Upwind contributions approximate type I terms by using the influence of waves generated in Riemann problems normal to each cell edge. A wave that emanates from the edge at $x = x_{i-1/2}$ travels a distance $u\,\Delta t$ into the upwind cell over one time step. The influence of this wave on the upwind cell average is computed by multiplying the wave strength $\boldsymbol{\mathcal{W}}_{i-1/2}$ by the fraction ν, of the cell volume that the wave occupies at the end of the time step

$$\nu = \frac{u\,\Delta t}{\Delta x}. \tag{2.29}$$

The upwind cell average (for $u > 0$) is modified by

$$\begin{aligned} \boldsymbol{Q}_i^{n+1} &= \boldsymbol{Q}_i^n - \frac{u\,\Delta t}{\Delta x}\boldsymbol{\mathcal{W}}_{i-1/2} \\ &= \boldsymbol{Q}_i^n - \frac{\Delta t}{\Delta x}\boldsymbol{\mathcal{A}}^+\boldsymbol{\Delta Q}_{i-1/2}. \end{aligned} \tag{2.30}$$

Using the definition (2.26) to incorporating the influence of multiple waves traveling in both directions as depicted in Figure 2.5, we write the standard first-order upwind method

$$\begin{aligned} \boldsymbol{Q}_i^{n+1} &= \boldsymbol{Q}_i^n - \frac{\Delta t}{\Delta x}\left(\boldsymbol{\mathcal{A}}^+\boldsymbol{\Delta Q}_{i-1/2} + \boldsymbol{\mathcal{A}}^-\boldsymbol{\Delta Q}_{i+1/2}\right) \\ &= \boldsymbol{Q}_i^n - \frac{\Delta t}{\Delta x}\boldsymbol{\Delta}_i. \end{aligned} \tag{2.31}$$

We use $\boldsymbol{\Delta}_i$ to denotes the influence of first-order fluctuations in $\mathcal{C}_i$

$$\boldsymbol{\Delta}_{\mathcal{C}} = \boldsymbol{\mathcal{A}}^+\boldsymbol{\Delta Q}_{i-1/2} + \boldsymbol{\mathcal{A}}^-\boldsymbol{\Delta Q}_{i+1/2}. \tag{2.32}$$

Conservation of type I terms

It was shown in Section 2.1 that a property of high resolution finite volume methods in flux difference form (2.5) is that they numerically conserve the $\boldsymbol{Q}_i^n$ that approximate components of $\boldsymbol{q}$. We have discussed the importance of maintaining such a conservative update. It is, therefore, necessary to show that the wave propagation update (2.32) can be cast into the flux difference form (2.5).

So far we have described how the waves that are generated in Riemann problems affect cell averages, but we have said little about the generation of the waves and the speeds at which they travel. If, for example, we are working with a nonlinear system, then waves strengths may be found by intersecting Hugoniot loci and integral curves, while adhering to physical entropy conditions. An exact solution, $\boldsymbol{Q}_{i-1/2}^{\star}$ along $x = x_{i-1/2}$ can be constructed using this information. Wave speeds can then be computed based on shock speeds or characteristic speeds, depending on the type of wave. As discussed in Section 2.2.1, with $\boldsymbol{Q}_{i-1/2}^{\star}$ known a natural choice for a numerical flux function would be $\boldsymbol{F}_{i-1/2}^n = \boldsymbol{f}(\boldsymbol{Q}_{i-1/2}^{\star})$. Conservation can then be guaranteed by defining

$$\boldsymbol{\mathcal{A}}^-\boldsymbol{\Delta Q}_{i-1/2} = \boldsymbol{F}_{i-1/2}^n - \boldsymbol{f}(\boldsymbol{Q}_{i-1}^n) \tag{2.33}$$

$$\boldsymbol{\mathcal{A}}^+\boldsymbol{\Delta Q}_{i-1/2} = \boldsymbol{f}(\boldsymbol{Q}_i^n) - \boldsymbol{F}_{i-1/2}^n, \tag{2.34}$$

so that across any interface the numerical flux exactly cancels and the exact flux difference remains.

If, however, the exact solution is too complicated, or too computationally expensive to compute, one may define a Jacobian matrix $A_{i-1/2}$ that linearizes the flux Jacobian at each cell interface. The nonlinear problem is then replaced by a linear one with a solution discussed in Section 2.2.1. Using a linearized Jacobian will yield a conservative method only if the condition

$$
\begin{aligned}
A_{i-1/2}\left(\boldsymbol{Q}_i - \boldsymbol{Q}_{i-1}\right) = \sum_{p=1}^{n_{eq}} \alpha^p_{i-1/2}\, A_{i-1/2}\, \boldsymbol{r}^p_{i-1/2} \\
&= \sum_{p=1}^{n_{eq}} \boldsymbol{s}^p_{i-1/2}\, \boldsymbol{\mathcal{W}}^p_{i-1/2} \\
&= \boldsymbol{f}(\boldsymbol{Q}_i) - \boldsymbol{f}(\boldsymbol{Q}_{i-1}),
\end{aligned}
\tag{2.35}
$$

where $\boldsymbol{r}^p$ are the eigenvectors and $\boldsymbol{s}^p_{i-1/2}$ are the eigenvalues of $A_{i-1/2}$ and the waves $\boldsymbol{\mathcal{W}}^p_{i-1/2} = \alpha^p\, \boldsymbol{r}^p$ with speeds $\boldsymbol{s}^p_{i-1/2}$ have been defined. This condition is imposed by defining a Jacobian matrix based on a Roe average defined in [69]. In this case when waves for a Riemann solution consisting of a single shock for a nonlinear scalar equation satisfy both (2.25) and (2.35), the Rankine-Hugoniot condition (2.23) is satisfied exactly as we would expect.

Conservation of type I terms in this case can be realized by defining a numerical flux denoted by $\boldsymbol{F}^n$ from (2.4) that approximates the time integral of the true flux $\boldsymbol{f}$ along a cell interface during a single time step. The numerical flux for the wave propagation algorithm at the left edge of $\mathcal{C}_i$ is written

$$
\boldsymbol{F}^n_{i-1/2} = \frac{1}{2}\left(\boldsymbol{f}(\boldsymbol{Q}_i) + \boldsymbol{f}(\boldsymbol{Q}_{i-1}) - \sum_{p=1}^{n_{eq}} |s^p_{i-1/2}| \boldsymbol{\mathcal{W}}^p_{i-1/2}\right). \tag{2.36}
$$

Using this definition of the numerical flux and the fluctuations (2.26) we can write

$$
\begin{aligned}
\boldsymbol{\Delta}_i &= \sum_p \left[s^p_{i-1/2}\right]^+ \boldsymbol{\mathcal{W}}^p_{i-1/2} + \sum_p \left[s^p_{i+1/2}\right]^- \boldsymbol{\mathcal{W}}^p_{i+1/2} \\
&= \sum_{p=1}^{n_{eq}} \frac{1}{2}\left(s^p_{i-1/2} + |s^p_{i-1/2}|\right) \boldsymbol{\mathcal{W}}^p_{i-1/2} + \sum_{p=1}^{n_{eq}} \frac{1}{2}\left(s^p_{i+1/2} - |s^p_{i+1/2}|\right) \boldsymbol{\mathcal{W}}^p_{i+1/2} \\
&= \boldsymbol{F}^n_{i+1/2} - \boldsymbol{F}^n_{i-1/2}.
\end{aligned}
\tag{2.37}
$$

The upwind update (2.31) for the wave propagation algorithm can then be written

$$
\boldsymbol{Q}^{n+1}_i = \boldsymbol{Q}^n_i - \sum_{k=1}^{n_d} \frac{\Delta t}{\Delta x}\left(\boldsymbol{F}^n_{i+1/2} - \boldsymbol{F}^n_{i-1/2}\right), \tag{2.38}
$$

which is in flux difference conservative form.

As long as waves are defined so that equation (2.35) holds, the wave propagation algorithm will generate conservative numerical solutions. We will also demonstrate that higher order corrections to these type I terms are also flux conservative, yielding a high-resolution flux conservative method when the definition of a flux function is appropriate.

Type II(a) terms: high resolution corrections

In the previous section, we demonstrated that the upwind contribution to the cell update can be viewed as computing the influence a wave has on a cell volume. Consider equation (2.27) with $u > 0$. The upwind contribution to the i^{th} cell average in this case was found to be

$$\boldsymbol{Q}_i^{n+1} = \boldsymbol{Q}_i^n - \frac{\Delta t}{\Delta x} u \boldsymbol{\mathcal{W}}_{i-1/2}. \tag{2.39}$$

Taking into account equation (2.25) we can write

$$-\frac{\Delta t}{\Delta x} u \boldsymbol{\mathcal{W}}_{i-1/2} = u \frac{\boldsymbol{Q}_i^n - \boldsymbol{Q}_{i-1}^n}{\Delta x} \tag{2.40}$$

which is a one-sided and first order accurate approximation to $u_{i-1/2} q_{,x}$. In order to capture higher order terms and produce a more accurate algorithm in regions of smooth solutions, the upwind contribution $\boldsymbol{\Delta}_i$ must be modified. However, the modifications must not destroy the conservative properties demonstrated in Section 2.3.1.

A correction flux is defined by

$$\tilde{\boldsymbol{F}}_{i-1/2} = \frac{1}{2} \sum_{p=1}^{n_{eq}} |s_{i-1/2}^p| \left(1 - \frac{\Delta t}{\Delta x} |s_{i-1/2}^p|\right) \tilde{\boldsymbol{\mathcal{W}}}_{i-1/2}^p \tag{2.41}$$

and implemented in a flux conservative way. The limited waves

$$\tilde{\boldsymbol{\mathcal{W}}}_{i-1/2}^p = \text{Limiter}(\boldsymbol{\mathcal{W}}_{i-1/2}^{(p)}, \boldsymbol{\mathcal{W}}_{I-1/2}^{(p)}), \tag{2.42}$$

have been introduced in the correction flux where

$$I = \begin{cases} i-1 & \text{if } s_{i-1/2}^p > 0 \\ i+1 & \text{if } s_{i-1/2}^p < 0 \end{cases}. \tag{2.43}$$

The wave-limiting function introduced here reduces the strength of the correction fluxes in regions of sharp gradients such as shock waves and contact discontinuities. Reducing the influence of higher order corrections limits well known oscillations produced by second order methods near such gradients. Details about the limiter functions used in calculations presented here can be found in [45], [46].

The modified update to the cell average can now be written

$$\boldsymbol{Q}_i^{n+1} = \boldsymbol{Q}_i^n - \frac{\Delta t}{\Delta x} \left(\boldsymbol{\Delta}_i + \tilde{\boldsymbol{F}}_{i+1/2} - \tilde{\boldsymbol{F}}_{i-1/2}\right). \tag{2.44}$$

The first term of this correction flux improves accuracy on the upwind approximation to $u\, q_{,x}$ by centralizing the difference. The second term gives a second-order accurate representation of type II(a) terms that look like $u^2\, q_{,xx}$. If these terms were not captured by the method then the numerical solution would smear the results. Finally, note that the high resolution correction fluxes introduced here are implemented in a flux difference so that the conservative properties of the update are kept.

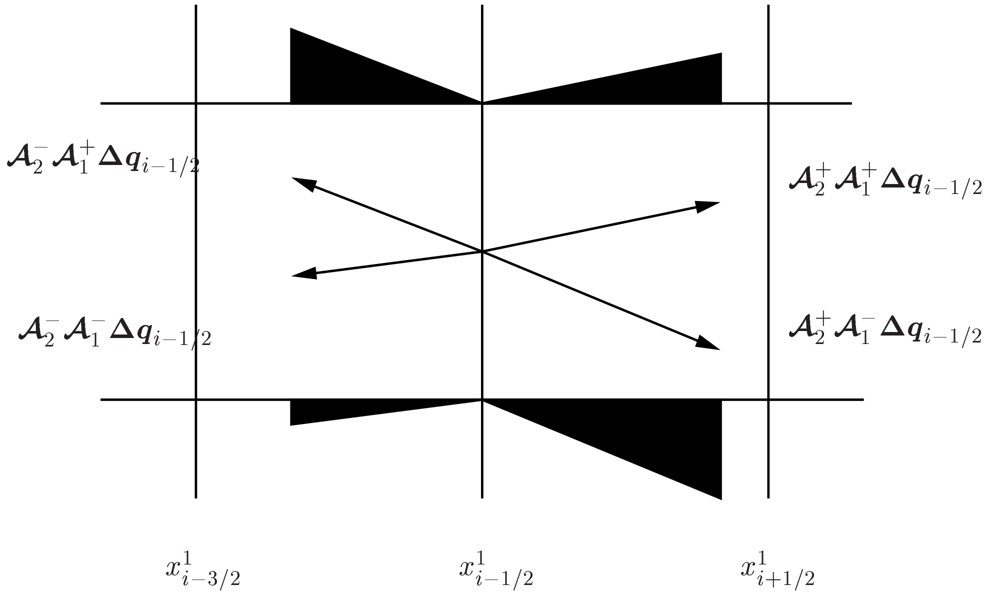

Figure 2.6: (a) A wave propagates in a multidimensional way that affects more cells than just the adjacent cells. (b) The correction triangles that result from the multidimensional propagation of waves.

2.3.2 Multidimensional algorithm

So far we have concentrated on one-dimensional contributions to the cell average. Many high resolution finite volume schemes base multidimensional cell updates on purely one-dimensional contributions and rely on dimensionally split time evolution to incorporate multidimensional effects. In reality the waves propagate in a multidimensional way and affect not only cell averages adjacent to the interface, but also any cell within the causal path of the waves over a time step. The influence of a wave traveling through a grid is depicted in figure 2.6 with all cells adjacent the the cell interface being affected. The standard wave propagation algorithm is an unsplit method that directly incorporates the effect of waves propagating in a multidimensional manner.

Consider the Taylor series of the multidimensional version of equation (2.27)

$$q_{,t} + u^k \, q_{,k} = 0, \tag{2.45}$$

which has the form

$$q(t + \Delta t) = q(t) - \Delta t \, \underbrace{u^k \, q_{,k}(t)}_{I} + \frac{1}{2}\Delta t^2 \, \underbrace{u^k \, u^j \, q_{,kj}(t)}_{II(a) \text{ and } II(b)} + \mathcal{O}(\Delta t^3). \tag{2.46}$$

A new type of term, denoted II(b), appears due to cross derivatives at second order. When $k = j$ the second order term is purely one dimensional and of Type I(a) that was discussed in the previous section. In this section we concentrate on terms of Type II(b) with $k \neq j$.

Type II(b) terms: Transverse propagation

Suppose that the wave travels through a grid with velocity $\vec{v} = u^1\vec{e}_{(1)} + u^2\vec{e}_{(2)}$ and $u^1, u^2 > 0$. The triangular portion of the wave that is entering cell $\mathcal{C}_{i,j+1}$ rather than $\mathcal{C}_{i,j}$ modifies the correction flux between these cells by

$$\tilde{\boldsymbol{F}}^{(2)}_{i,j+1/2} \rightarrow \tilde{\boldsymbol{F}}^{(2)}_{i,j+1/2} - \frac{\Delta t}{2\,\Delta\, x^1}\, u^1\, u^2 \left(\boldsymbol{Q}^n_{ij} - \boldsymbol{Q}^n_{i-1j}\right). \tag{2.47}$$

Notice that we once again use the notation that an subscript index or a superscript index with braces around it indicates a spatial vector in that direction (i.e. $\tilde{\boldsymbol{F}}^{(2)}_{i,j}$ is the correction flux for cell $\mathcal{C}_{i,j}$ in the x^2 direction). This modification can be viewed as decomposing the right-going fluctuation into fluctuations traveling in the transverse direction.

A system of equations typically has both a left-going fluctuation $\boldsymbol{\mathcal{A}}^-_k\boldsymbol{\Delta Q}_{ij}$, and a right-going fluctuation $\boldsymbol{\mathcal{A}}^+_k\boldsymbol{\Delta Q}_{ij}$ for a sweep through the grid in the x^k direction. Each of these will be split into an up-going transverse piece $\boldsymbol{\mathcal{A}}^+_2\boldsymbol{\mathcal{A}}^*_1\boldsymbol{\Delta q}_{ij}$ and a down-going transverse piece $\boldsymbol{\mathcal{A}}^-_2\boldsymbol{\mathcal{A}}^*_1\boldsymbol{\Delta q}_{ij}$. These transverse fluctuations create four triangular corrections modifying the cell updates in the four neighboring cells as indicated in figure 2.6. In general, the transverse fluctuations are used to modify the four neighboring fluxes according to

$$\tilde{\boldsymbol{F}}^{(2)}_{i,j+1/2} \rightarrow \tilde{\boldsymbol{F}}^{(2)}_{i,j+1/2} - \frac{1}{2}\frac{\Delta t}{\Delta x^1}\boldsymbol{\mathcal{A}}^+_2\boldsymbol{\mathcal{A}}^+_1\boldsymbol{\Delta q}_{i-1/2} \tag{2.48}$$

$$\tilde{\boldsymbol{F}}^{(2)}_{i,j-1/2} \rightarrow \tilde{\boldsymbol{F}}^{(2)}_{i,j-1/2} - \frac{1}{2}\frac{\Delta t}{\Delta x^1}\boldsymbol{\mathcal{A}}^-_2\boldsymbol{\mathcal{A}}^+_1\boldsymbol{\Delta q}_{i-1/2} \tag{2.49}$$

$$\tilde{\boldsymbol{F}}^{(2)}_{i-1,j+1/2} \rightarrow \tilde{\boldsymbol{F}}^{(2)}_{i-1,j+1/2} - \frac{1}{2}\frac{\Delta t}{\Delta x^1}\boldsymbol{\mathcal{A}}^+_2\boldsymbol{\mathcal{A}}^-_1\boldsymbol{\Delta q}_{i-1/2} \tag{2.50}$$

$$\tilde{\boldsymbol{F}}^{(2)}_{i-1,j-1/2} \rightarrow \tilde{\boldsymbol{F}}^{(2)}_{i-1,j-1/2} - \frac{1}{2}\frac{\Delta t}{\Delta x^1}\boldsymbol{\mathcal{A}}^-_2\boldsymbol{\mathcal{A}}^-_1\boldsymbol{\Delta q}_{i-1/2}, \tag{2.51}$$

so that the form of the full high resolution multidimensional update is

$$\boldsymbol{Q}^{n+1}_{\mathcal{C}} = \boldsymbol{Q}^n_{\mathcal{C}} - \sum_{k=1}^{n_d}\frac{\Delta t}{\Delta x^k}\left(\boldsymbol{\Delta}^k_{\mathcal{C}} + \tilde{\boldsymbol{F}}^{(k)}_{i+1/2} - \tilde{\boldsymbol{F}}^{(k)}_{i-1/2}\right) \tag{2.52}$$

where we denote the finite volume cell by $\mathcal{C}$, the sum is over the n_d spatial dimensions and $\boldsymbol{\Delta}^k_{\mathcal{C}}$ is the first order update in the x^k direction.